A multi-term solution of the nonconservative Boltzmann equation for the analysis of temporal and spatial non-local effects in charged-particle swarms in electric and magnetic fields

2011 Plasma Sources Sci. Technol. 20 024013

(http://iopscience.iop.org/0963-0252/20/2/024013)

Plasma Sources Sci. Technol. **20** (2011) 024013 (15pp) doi:10.1088/0963-0252/20/2/024013

A multi-term solution of the nonconservative Boltzmann equation for the analysis of temporal and spatial non-local effects in charged-particle swarms in electric and magnetic fields

S Dujko[1,2,3], R D White[2], Z Lj Petrović[1] and R E Robson[2]

[1] Institute of Physics, University of Belgrade, PO Box 68, Zemun, Belgrade, Serbia
[2] ARC Centre for Antimatter-Matter Studies, School of Mathematics, Physics and Information Technology, James Cook University, Townsville 4810, Australia
[3] Centre for Mathematics and Computer Science (CWI), PO Box 94079, 1090 GB Amsterdam, The Netherlands

E-mail: sasa.dujko@ipb.ac.rs

Received 20 September 2010, in final form 25 February 2011
Published 1 April 2011
Online at stacks.iop.org/PSST/20/024013

Abstract
A multi-term solution of the Boltzmann equation has been developed and used to investigate the temporal and spatial relaxation of charged-particle swarms and associated phenomena induced by non-local effects under the influence of electric and magnetic fields crossed at arbitrary angles when nonconservative collisions are operative. The hierarchy resulting from a spherical harmonic decomposition of the Boltzmann equation in both the hydrodynamic and non-hydrodynamic regimes is solved numerically by representing the speed dependence of the phase-space distribution function in terms of an expansion in Sonine polynomials about a variety of Maxwellian based weighting functions. Temporal and spatial relaxation profiles of various charged-particle swarm transport properties are presented for certain model and real gases over a range of field strengths and angles between the fields. It was found that the magnetic field strength and angle between the fields have an ability to control the relaxation process: in general, these parameters can be used to enhance or suppress the oscillatory features in the relaxation profiles of various transport properties. The explicit and implicit effects of nonconservative collisions on the drift and diffusion elements in varying configurations of radio-frequency electric and magnetic fields are considered using physical arguments.

(Some figures in this article are in colour only in the electronic version)

1. Introduction

Non-equilibrium, low-temperature plasma discharges sustained and controlled by electric and magnetic fields are widely used routinely in many scientific and industrial applications [1, 2]. It is well known that within these discharges the electric and magnetic fields vary in space, time and orientation depending on the type of discharge. Consequently, the transport of electrons and ions within these discharges is complex. In general, transport/plasma properties are non-local in both space and time, i.e. transport properties at a given point are no longer a function of instantaneous local fields. While there has been a considerable amount of research into temporal and spatial non-locality of electron transport for electric fields only, the study of such effects including an additional magnetic field is limited. This may be due in part to the unavoidable additional complexity associated with introducing the magnetic field into the theories and simulations. When one

requires high accuracy this additional complexity is generally unavoidable.

Since the mid- to late-1990s the theoretical analysis of charged-particle transport processes in neutral gases in the presence of electric and magnetic fields has advanced considerably. For electron swarms in crossed electric and magnetic fields, progress was stimulated by the desire to overcome the accuracy limitations of the two-term approximation for solving the Boltzmann equation and various types of equivalent/effective field approximations often employed to describe the impact of a magnetic field on the transport. While effective and equivalent field theories [3–5] including fluid treatments [6] can generally identify much of the physics present in the problem, when high accuracy is demanded multi-term Boltzmann equation solutions and Monte Carlo simulations are inevitable [7, 8]. The first systematic multi-term analysis for electron swarms under hydrodynamic conditions in the presence of uniform dc electric and magnetic fields was given by Ness [9] and since then a considerable number of papers has been published in a relatively short time. The situation up to 2002 was reviewed in [10] where a unified multi-term theory for solving the Boltzmann equation valid for both electrons and ions in the presence of time-dependent electric and magnetic fields was presented. This theory was recently employed to study the influence of an orthogonal magnetic field on the transient behavior of the diagonal diffusion tensor elements for swarms undergoing conservative collisions only [11, 12]. Since ionization plays a vital role in plasma maintenance any transport theory must include rate coefficients, and correctly account for the effects of nonconservative collisions on drift and diffusion. When a magnetic field is present and/or when the fields vary in time, space, phase and orientations transport data cannot simply be obtained from an adaptation of dc electric field results. A multitude of kinetic phenomena induced by the temporal non-locality in electron transport in radio-frequency electric and magnetic fields have been observed by a Monte Carlo simulation technique [8, 13, 14] that are generally inexplicable through the use of steady-state dc transport theory. With these remarks as background, we extend the previous theory outlined in [10–12] and in this work we present a theoretical and numerical investigation of hydrodynamic charged-particle swarms in neutral gases under the influence of dc and ac electric and magnetic fields when nonconservative collisions are operative with applications of non-equilibrium magnetized plasma discharges to plasma processing, gas laser discharges and drift chambers for detection particles in mind. Preliminary and some illustrative examples have already been published in [15] while in [16] this theory has been systematically benchmarked in varying configurations of electric and magnetic fields against results obtained by a Monte Carlo simulation technique.

We begin this paper with a brief review of a multi-term theory for solving the Boltzmann equation valid for both electrons and ions under the time-dependent hydrodynamic and steady-state non-hydrodynamic conditions when electric and magnetic fields are crossed at arbitrary angles and when nonconservative collisional processes are operative. We focus on two situations: (i) temporal relaxation and transport of the electrons under time-dependent hydrodynamic conditions and (ii) spatial relaxation of the electrons under steady-state non-hydrodynamic conditions. In addition to the Boltzmann equation analysis, our Monte Carlo simulation code specifically developed to study the spatial relaxation of electrons in an idealized SST experiment in the presence of nonconservative collisions [17] is applied to test and benchmark results obtained via a Boltzmann equation analysis. After giving brief reviews of theoretical methods, we then give numerical examples for various cases of special interest, highlighting recent new results.

2. Theory

The behavior of charged-particle swarms in gases under the influence of electric and magnetic fields is described by the phase-space distribution function $f(\boldsymbol{r}, \boldsymbol{c}, t)$ representing the solution of the Boltzmann equation

$$\frac{\partial f}{\partial t} + \boldsymbol{c} \cdot \frac{\partial f}{\partial \boldsymbol{r}} + \frac{q}{m} [\boldsymbol{E} + \boldsymbol{c} \times \boldsymbol{B}] \cdot \frac{\partial f}{\partial \boldsymbol{c}} = -J(f, f_0), \qquad (1)$$

where $\boldsymbol{r}$ and $\boldsymbol{c}$ denote the position and velocity co-ordinates, q and m are the charge and mass of the swarm particle and t is time. The electric and magnetic fields are assumed spatially homogeneous with magnitudes E and B, respectively. In what follows, we employ a co-ordinate system in which $\boldsymbol{E}$ defines the z-direction while $\boldsymbol{B}$ lies in the y–z plane, making an angle ψ with respect to the $\boldsymbol{E}$. Swarm conditions are assumed to apply and $J(f, f_0)$ denotes the rate of change of f due to binary collisions with the neutral molecules only. The original Boltzmann collision operator [18] and its semiclassical generalization [19] are used for elastic and inelastic processes, respectively. The attachment and ionization collision operators employed are detailed in [20].

2.1. Representation of the velocity dependence

The velocity dependence of f is represented in terms of a combined spherical harmonic and Sonine polynomial expansion about a Maxwellian at a temperature T_b:

$$f(\boldsymbol{r}, \boldsymbol{c}, t) = w(\alpha, c) \sum_{\nu=0}^{\infty} \sum_{l=0}^{\infty} \sum_{m=-l}^{l} F(\nu l m | \boldsymbol{r}, \alpha, t) R_{\nu l}(\alpha c) \times Y_m^{[l]}(\hat{\boldsymbol{c}}), \qquad (2)$$

where

$$w(\alpha, c) = \left(\frac{\alpha^2}{2\pi}\right)^{3/2} \exp\left\{\frac{-\alpha^2 c^2}{2}\right\}, \qquad (3)$$

$$R_{\nu l}(\alpha c) = N_{\nu l} \left(\frac{\alpha c}{\sqrt{2}}\right)^l S_{l+1/2}^{(\nu)}\left(\frac{\alpha^2 c^2}{2}\right), \qquad (4)$$

$$N_{\nu l}^2 = \frac{2\pi^{3/2} \nu!}{\Gamma(\nu + l + 3/2)}. \qquad (5)$$

Here $Y_m^{[l]}(\hat{\boldsymbol{c}})$ are spherical harmonics, $\hat{\boldsymbol{c}}$ denotes the angles of $\boldsymbol{c}$, $S_{l+1/2}^{(\nu)}(\frac{\alpha^2 c^2}{2})$ are Sonine polynomials and $\alpha^2 = \frac{m}{kT_b}$.

The modified Sonine polynomials satisfy the orthonormality relation

$$\int_0^\infty w(\alpha, c) R_{\nu' l'}(\alpha c) R_{\nu l}(\alpha c) c^2 dc = \delta_{\nu' \nu} \delta_{l' l}. \tag{6}$$

The various properties of the moments due to symmetry and reality considerations carry over from the steady-state theory and are described in [21, 22]. It should be emphasized, however, that for electric and magnetic fields crossed at an arbitrary angle, the moments of the distribution function are generally complex.

Using the appropriate orthogonality relations the following system of coupled differential equations for the moments $F(\nu lm; \boldsymbol{r}, t, \alpha)$ is generated:

$$\begin{aligned}
&\sum_{\nu'=0}^{\infty} \sum_{l'=0}^{\infty} \sum_{m'=-l'}^{l'} \Bigg[\left(\frac{\partial}{\partial t} \delta_{\nu\nu'} + n_0 J^l_{\nu\nu'}(\alpha) \right) \delta_{l'l} \delta_{m'm} \\
&\quad + \mathrm{i} \frac{qE}{m} \alpha (l' m 10 | lm) \langle \nu l || K^{[1]} || \nu' l' \rangle \delta_{m'm} \\
&\quad + \frac{qB}{m} \Bigg\{ \sqrt{(l-m)(l+m+1)} \frac{\sin\psi}{2} \delta_{m'm+1} \\
&\quad - \sqrt{(l+m)(l-m+1)} \frac{\sin\psi}{2} \delta_{m'm-1} - \mathrm{i} m \cos\psi \delta_{mm'} \Bigg\} \\
&\quad \times \delta_{l'l} \delta_{\nu'\nu} - \mathrm{i} \frac{1}{\alpha} (l' m 10 | lm) \langle \nu l || \alpha c^{[1]} || \nu' l' \rangle \delta_{m'm} \nabla \Bigg] \\
&\quad \times F(\nu' l' m'; \boldsymbol{r}, t, \alpha) = 0, \qquad (\nu, l) = 0, 1, 2, \ldots, \infty, \quad m = -l, -l+1, \ldots, l-1, l,
\end{aligned} \tag{7}$$

where n_0 is the neutral gas number density while $(l' m 10 | lm)$ is a Clebsch–Gordan coefficient. The reduced matrix elements $J^l_{\nu\nu'}(\alpha)$, $\langle \nu l || \alpha c^{[1]} || \nu' l' \rangle$ and $\langle \nu l || K^{[1]} || \nu' l' \rangle$ of the collision operator, velocity and velocity derivative are given by (11), (12*a*) and (12*b*) of [20], respectively. For further details the reader is referred to [10, 15].

2.2. Representation of the spatial dependence

The treatment of the spatial dependence of the phase-space distribution function is dependent on the conditions under which the experiment is performed.

Hydrodynamic regime. In carefully controlled swarm experiments, spatial gradients are designed to be small so that the *hydrodynamic regime* in general prevails, and the space-time dependence can be projected onto the number density [23]. In this regime, the distribution function can be expressed in terms of a linear functional of $n(\boldsymbol{r}, t)$, usually taken to be a density gradient expansion (see equation (8)). Experiments may be analyzed via solution of the diffusion equation, and transport coefficients extracted accordingly. Similar conditions can often be found far away from the electrodes in the bulk of a weakly ionized non-equilibrium plasma where the fields are almost spatially homogeneous. In any case, for studies of transport in the hydrodynamic regime the spatial dependence is projected onto the number density through a time-dependent density gradient expansion:

$$\begin{aligned}
F(\nu lm | \boldsymbol{r}, t, \alpha) = &\sum_{s=0}^{\infty} \sum_{\lambda=0}^{\infty} \sum_{\mu=-\lambda}^{\lambda} F(\nu lm | s\lambda\mu; t, \alpha) \\
&\times G^{(s\lambda)}_{\mu} n(\boldsymbol{r}, t),
\end{aligned} \tag{8}$$

where $G^{(s\lambda)}_{\mu} n(\boldsymbol{r}, t)$ is the irreducible gradient tensor operator [20]. Substituting into (7) and equating coefficients of $G^{(s\lambda)}_{\mu} n(\boldsymbol{r}, t)$ yields the following hierarchy of equations for the calculation of time-dependent transport coefficients:

$$\begin{aligned}
&\sum_{\nu'=0}^{\infty} \sum_{l'=0}^{\infty} \sum_{m'=0}^{\infty} \Bigg[(n_0 J^l_{\nu\nu'}(\alpha) + R_a \delta_{\nu\nu'}) \delta_{ll'} \delta_{mm'} \\
&\quad + \mathrm{i} \frac{qE}{m} \alpha (l' m 10 | lm) \langle \nu l || K^{[1]}(\alpha) || \nu' l' \rangle \\
&\quad + \frac{qB}{m} \Bigg\{ \sqrt{(l-m)(l+m+1)} \frac{\sin\psi}{2} \delta_{m'm+1} \\
&\quad - \sqrt{(l+m)(l-m+1)} \frac{\sin\psi}{2} \delta_{m'm-1} \\
&\quad - \mathrm{i} m \cos\psi \delta_{m'm} \Bigg\} \delta_{\nu\nu'} \delta_{ll'} - n_0 J^0_{0\nu'}(\alpha) F(\nu lm | 000) \\
&\quad \times (1 - \delta_{s0} \delta_{\lambda 0} \delta_{\mu 0}) \delta_{l'0} \delta_{m'0} \Bigg] \\
&\quad \times F(\nu' l' m' | s\lambda\nu) = X(\nu lm | s\lambda\nu),
\end{aligned} \tag{9}$$

where R_a is the net creation rate given by

$$R_a = n_0 \sum_{\nu=0}^{\infty} J^0_{0\nu}(\alpha) F(\nu lm | 000). \tag{10}$$

The matrix elements of the collision matrix $J^0_{0\nu}$ are non-zero only when ionization and/or attachment processes are operative. The spatially homogeneous member of the hierarchy (9) and (10) constitute a non-linear system of equations for the spatially homogeneous moments $F(\nu lm | 000)$. This system is solved iteratively using the similar method initially developed by Ness and co-workers [9, 10, 24, 25].

The explicit expressions for the RHS are given in [16]. Discretizing in time using an implicit finite difference scheme converts the hierarchy of systems of coupled differential equations into a hierarchy of coupled matrix equations. In the absence of nonconservative collisions, it is sufficient only to solve the members of the hierarchy up to first order in the density gradients, to determine all quantities of interest. However, in order to investigate the explicit influence of nonconservative collisions on both the drift and diffusion a second-order density gradient is required and the following members of the hierarchy (9) must be considered: $(s, \lambda, \mu) = (0,0,0), (1,1,0), (1,1,1), (2,0,0), (2,2,0), (2,2,1), (2,2,2)$. The bulk drift velocity components are related to the calculated moments via

$$\begin{aligned}
W_x = &\frac{\sqrt{2}}{\alpha} \mathrm{Im}\{F(011|000; \alpha)\} \\
&- \sqrt{2} \sum_{\nu'=0}^{\infty} n_0 J^0_{0\nu'} \mathrm{Im}\Big\{ F(\nu' 00 | 111; \alpha) \Big\},
\end{aligned} \tag{11}$$

$$W_y = \frac{\sqrt{2}}{\alpha}\mathrm{Re}\Big\{F(01-1|000;\alpha)\Big\} + \sqrt{2}\sum_{\nu'=0}^{\infty} n_0 J^0_{0\nu'}\mathrm{Re}\Big\{F(\nu'00|111;\alpha)\Big\}, \quad (12)$$

$$W_z = -\frac{1}{\alpha}\mathrm{Im}\Big\{F(010|000;\alpha)\Big\} + \sum_{\nu'=0}^{\infty} n_0 J^0_{0\nu'}\mathrm{Im}\Big\{F(\nu'00|110;\alpha)\Big\}. \quad (13)$$

while the bulk diagonal elements of the diffusion tensor are given by

$$D_{xx} = -\frac{1}{\alpha}\Big[\mathrm{Re}\Big\{F(011|111;\alpha)\Big\} - \mathrm{Re}\Big\{F(01-1|111;\alpha)\Big\}\Big] - \sum_{\nu'=0}^{\infty} n_0 J^0_{0\nu'}\Big[\frac{1}{\sqrt{3}}F(\nu'00|200;\alpha) + \frac{1}{\sqrt{6}}F(\nu'00|220;\alpha) - \mathrm{Re}\Big\{F(\nu'00|222;\alpha)\Big\}\Big], \quad (14)$$

$$D_{yy} = -\frac{1}{\alpha}\Big[\mathrm{Re}\Big\{F(011|111;\alpha)\Big\} + \mathrm{Re}\Big\{F(01-1|111;\alpha)\Big\}\Big] - \sum_{\nu'=0}^{\infty} n_0 J^0_{0\nu'}\Big[\frac{1}{\sqrt{3}}F(\nu'00|200;\alpha) + \frac{1}{\sqrt{6}}F(\nu'00|220;\alpha) + \mathrm{Re}\Big\{F(\nu'00|222;\alpha)\Big\}\Big], \quad (15)$$

$$D_{zz} = -\frac{1}{\alpha}F(010|110;\alpha) - \sum_{\nu'=0}^{\infty} n_0 J^0_{0\nu'}\Big[\frac{1}{\sqrt{3}}F(\nu'00|200;\alpha) - \sqrt{\frac{2}{3}}F(\nu'00|220;\alpha)\Big]. \quad (16)$$

The terms involving the summations in the drift velocity components and diagonal elements of the diffusion tensor represent the explicit effects of nonconservative collisions while the rest constitute the flux contribution. The readers are referred to [26, 27] for a detailed discussion of the transport coefficient definitions. The bulk transport coefficients are usually tabulated in the literature but for some aspects of plasma modeling the flux data are required [27]. The most appropriate procedure would be to use the experimental swarm data (e.g. bulk values) for the analysis of the validity of the cross section and then to calculate the flux quantities which are necessary as input data in fluid modeling of plasma discharges as detailed by Robson *et al* [27]. It must be emphasized that in some cases the bulk and flux transport coefficients may exhibit completely different qualitative behavior, as in cases of negative absolute electron flux mobility (but not bulk mobility) for strongly attaching gases [28, 29] and negative differential conductivity (NDC) for positron bulk drift velocity (but not flux drift velocity) [30]. In the absence of nonconservative collisions, these two sets of coefficients coincide. We note Re{ } and Im{ }, respectively, represent the real and imaginary parts of the moments. The spatially averaged mean energy is given by

$$\varepsilon = \tfrac{3}{2}kT_b\big[1 - \sqrt{\tfrac{2}{3}}F(100|000;\alpha)\big]. \quad (17)$$

while the energy gradient vector components are given by

$$\gamma_x = \tfrac{3}{2}kT_b\big[\tfrac{2}{\sqrt{3}}\mathrm{Im}\big\{F(100|111;\alpha)\big\}\big], \quad (18)$$

$$\gamma_y = \tfrac{3}{2}kT_b\big[-\tfrac{2}{\sqrt{3}}\mathrm{Re}\big\{F(100|111;\alpha)\big\}\big], \quad (19)$$

$$\gamma_z = \tfrac{3}{2}kT_b\big[-\sqrt{\tfrac{2}{3}}\mathrm{Im}\big\{F(100|110;\alpha)\big\}\big]. \quad (20)$$

Other transport properties of interest for this work including the temperature tensor components and spatially homogeneous distribution function are defined in our previous publications [10, 15, 21, 22].

Non-hydrodynamic regime. In many discharges the existence of sources, boundaries and/or spatially varying fields can give rise to *non-hydrodynamic* behavior. In this case, the spatial dependence must be treated explicitly. Here we use a second-order finite differencing scheme with appropriate modifications at the boundaries to solve the hierarchy (7). The quantities of interest in terms of the calculated moments are

$$n(z) = F(000;\alpha,z), \quad (21)$$

$$\varepsilon(z) = \frac{3}{2}kT_b\left[1 - \sqrt{\frac{2}{3}}\frac{F(100;\alpha,z)}{F(000;\alpha,z)}\right], \quad (22)$$

$$v_z(z) = -\frac{1}{\alpha}\frac{\mathrm{Im}[F(010;\alpha,z)]}{F(000;\alpha;z)}, \quad (23)$$

$$v_x(z) = \frac{\sqrt{2}}{\alpha}\frac{\mathrm{Im}[F(011;\alpha,z)]}{F(000;\alpha;z)}, \quad (24)$$

$$v_y(z) = \frac{\sqrt{2}}{\alpha}\frac{\mathrm{Re}[F(011;\alpha,z)]}{F(000;\alpha;z)}. \quad (25)$$

As previously emphasized, our Monte Carlo code has been used for a verification of the results obtained under hydrodynamic conditions. The reader is referred to a recent paper [17] for a detailed discussion how to sample data under SST conditions when the ionization and/or attachment significantly alter the spatial relaxation of the electrons.

3. Results and discussion

In this section the theory outlined in the previous section is applied to a series of model and real gases when nonconservative collisions are present under both the hydrodynamic and non-hydrodynamic conditions. The motivation for employing model gases lies in the fact that through the use of simple forms of cross sections we can isolate and elucidate fundamental physical processes which govern the specific behavior of electron swarm for a given set of simulation conditions. In addition, the analytical form of the cross sections provides no ambiguity and uncertainty generated by the complicated structure of real cross sections. It must be emphasized, however, that our theory and associated code are equally valid for real cross sections, as is also demonstrated here.

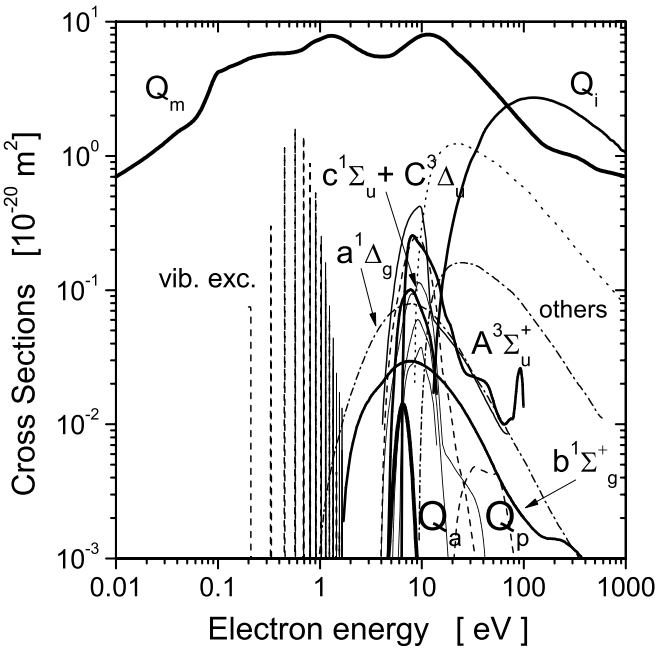

Figure 1. Electron impact cross sections for molecular oxygen used in this study [25, 31, 32].

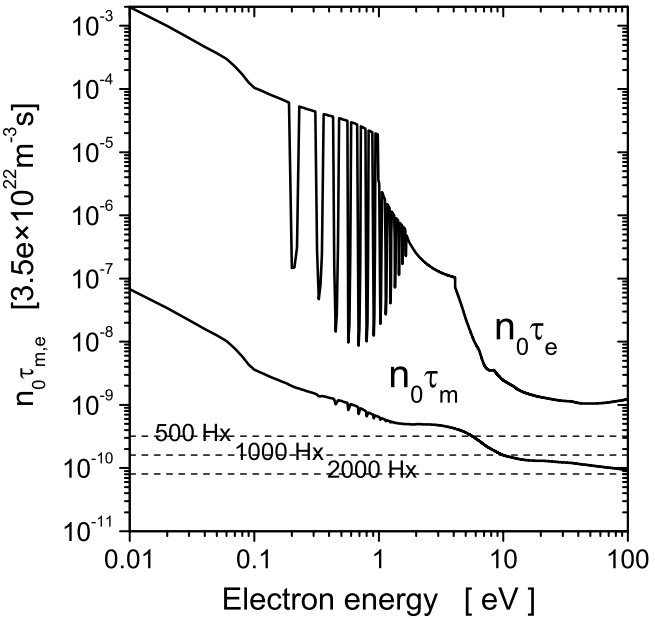

Figure 2. Comparison of the reduced cyclotron period for various B/n_0 (solid horizontal lines) with the reduced timescales for momentum and energy relaxation as a function of energy.

In this section we do not attempt a detailed analysis of transport properties and distribution function components for various gases and their variation with applied field frequency, electric and magnetic field strengths and field orientations. Such details are left to a subsequent paper and can in any case be found in [22]. Rather it is the aim of this section to present results which highlight the errors associated with certain approximations commonly employed in this field, alluded to in the earlier sections. In general in our theories and associated codes are accurate to at least 1%.

3.1. Temporal relaxation

In this section we consider the response of macroscopic transport properties to the application of a magnetic field for electrons in molecular oxygen under hydrodynamic conditions. The cross sections for electron scattering in molecular oxygen detailed in [25, 31, 32] are considered in this study and displayed in figure 1. The large cross sections for vibrational excitations in O_2 produce a large asymmetry in velocity space which makes the two-term approximation for solving the Boltzmann equation inadequate for the analysis of transient behavior of various transport parameters from the initial to the final time where all transport parameters have reached their steady-state values. A value of $l_{\max} = 4$ was required in order to achieve convergence to within 1% for the various transport properties of interest. This work is an extension of the work in [11] to consider spatially inhomogeneous transport coefficients in the presence of nonconservative collisions and for an arbitrary field configuration. The initial conditions represent the steady-state magnetic field-free case where the electron swarm is acted on solely by a dc electric field ($E/n_0 = 270\,\mathrm{Td}$, $B/n_0 = 0\,\mathrm{Hx}$; $1\,\mathrm{Td} = 10^{-21}\,\mathrm{V\,m^2}$, $1\,\mathrm{Hx} = 10^{-27}\,\mathrm{Tm^3}$). At time $t = 0$, a crossed magnetic field is switched on (electric field is unaltered) and the relaxation properties of the swarm are followed as a function of time (normalized time $n_0 t$). These steady-state results are well documented [25] and our results are in agreement with these previous calculations.

To understand the main aspects of the temporal relaxation of electron swarm in electric and magnetic fields, the characteristic timescales for momentum (τ_m) and energy (τ_e) relaxation must be compared with the gyration period ($\tau = \Omega^{-1}$, where Ω is the gyro-frequency). These characteristic timescales for momentum and energy relaxation can be found from the corresponding momentum (ν_m) and energy (ν_e) dissipation frequencies [1, 47]:

$$\nu_\mathrm{m}(\epsilon) = \sqrt{\frac{2}{m}}\epsilon^{1/2}\left(n_0 Q_\mathrm{m}(\epsilon) + \sum_i n_0 Q_i^\mathrm{tot}(\epsilon)\right), \tag{26}$$

$$\nu_\mathrm{e}(\epsilon) = \sqrt{\frac{2}{m}}\epsilon^{1/2}\left(2\frac{m}{m_0}n_0 Q_\mathrm{m}(\epsilon) + \sum_i n_0 Q_i^\mathrm{tot}(\epsilon)\frac{\Delta\epsilon_i^\mathrm{tot}}{\epsilon}\right), \tag{27}$$

where $m_0, \epsilon, n_0, Q_\mathrm{m}, Q_i^\mathrm{tot}$ and $\Delta\epsilon_i^\mathrm{tot}$ denote the mass of neutral molecule, the electron energy, the gas number density, the momentum transfer cross section for elastic collisions, the total inelastic cross section and the energy loss of the lth inelastic process. It is evident from the definition of the dissipation frequencies that these characteristic timescales will vary by virtue of the variation of the swarm's energy distribution. Similar observations have been made for the magnetic field-free case [1, 33]. The characteristic timescales are shown in figure 2. We observe that the momentum dissipation occurs much faster than the energy dissipation due to the fact that cross section for momentum transfer in elastic collisions dominate the total cross section for inelastic collisions. When inelastic collisions start to play a significant role, the efficiency of energy

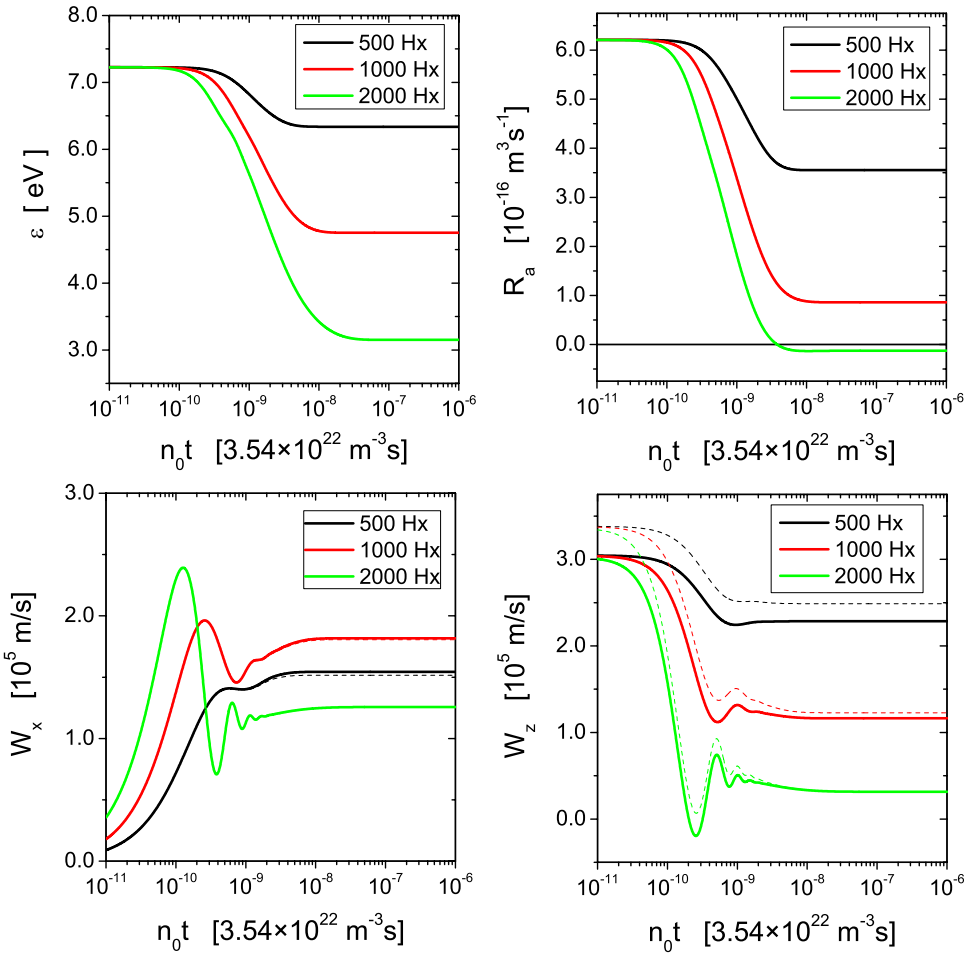

Figure 3. Temporal relaxation of the mean energy, the effective ionization coefficient and drift velocity components as a function of B/n_0 in a crossed field configuration for electrons in molecular oxygen (full line: flux; dashed line: bulk).

dissipation becomes more pronounced. The application of magnetic field generally decreases the mean energy of the swarm and hence both τ_m and τ_e increase as a result. Figure 2 emphasizes (particularly when magnetic field is present) that the energy dependences of τ_m and τ_e have to be taken into account in detail and cannot be replaced by some constant effective quantities. In general, these characteristic timescales are clearly evident in the relaxation profiles shown below.

Figure 3 displays the temporal relaxation of the mean energy, effective ionization coefficient and drift velocity components for electrons in molecular oxygen in a crossed field configuration. In figure 4 we show the temporal relaxation of the diagonal elements of the diffusion tensor and z-component of the gradient energy vector. In particular, the gradient energy vector [34] plays a key role in physical understanding of the effects of nonconservative collisions on electron transport coefficients. This quantity represents the first-order spatial variation of the average energy along the swarm. Apart from studies of the so-called explicit and implicit effects of nonconservative collisions on transport coefficients, this quantity plays an important role for conversion of transport data under the steady-state Townsend conditions into their hydrodynamic values [17]. The various transport properties display profiles that are either monotonic relaxation or damped periodic relaxation. For quantities such as the mean energy or the diffusion coefficient $n_0 D_{yy}$, relaxation is always monotonic and occurs on the timescale governed by τ_e. In contrast, the relaxation profiles of the drift and diffusion coefficients exhibit a transition from monotonic decay to damped periodic decay as the magnetic field strength is increased to values where $\tau \leqslant \tau_m$. For the damped periodic profiles, the oscillations are on the timescale of the gyro-orbits τ and the envelope decays on a timescale of τ_m together with a further relaxation on the timescale of τ_e. The existence of the additional oscillatory behavior in the relaxation profiles is an imprint of the collective gyrations of the electrons damped by collisions that exchange energy and momentum. Perhaps the most striking phenomenon is the existence of transiently negative excursions of the diffusion tensor elements in both the $\boldsymbol{E}$ and $\boldsymbol{E} \times \boldsymbol{B}$ directions. The existence of transiently negative diagonal diffusion elements in swarms was observed in CO_2 [15] as well as in rf fields [35] and is explained in greater detail in [11, 22]. These transient properties are quite general and have been previously observed for a range of model and real gases [11, 12, 36].

Considering the effects of nonconservative processes on the relaxation profiles we observe the following interesting points. In the early stage of the relaxation process there is a

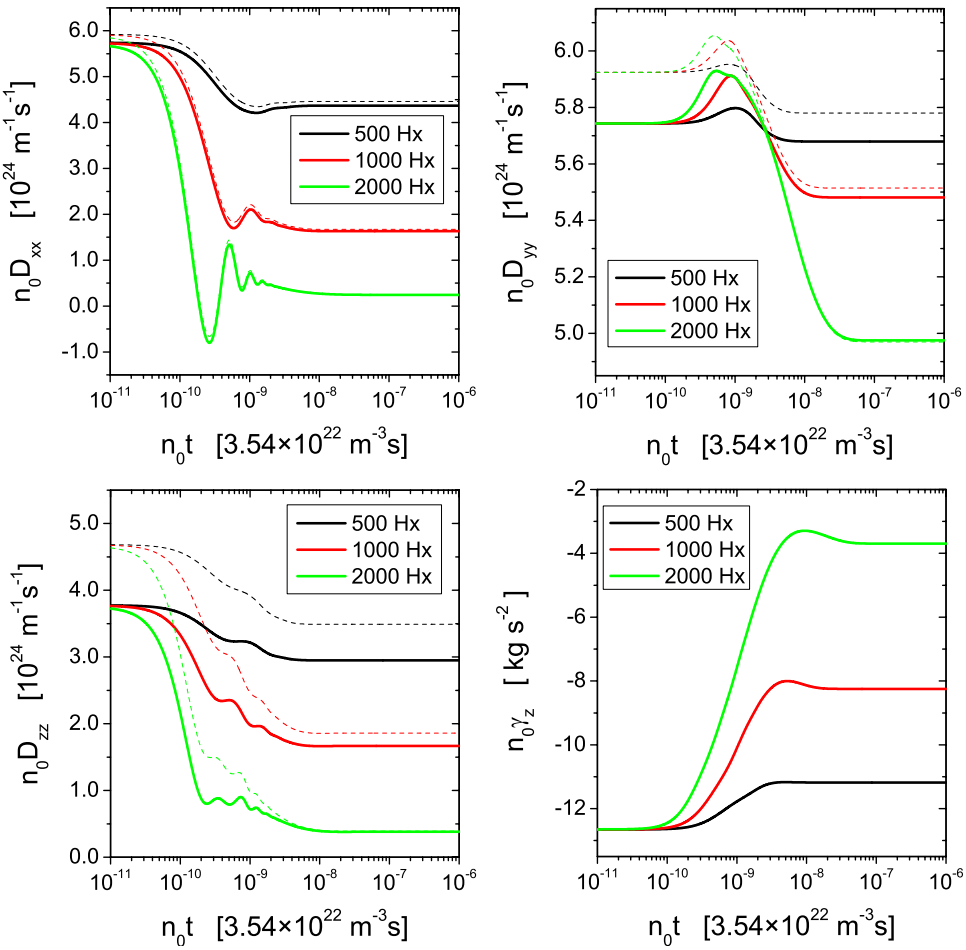

Figure 4. Temporal relaxation of the diagonal elements of the diffusion tensor and z-component of the gradient energy vector as a function of B/n_0 in a crossed field configuration for electrons in molecular oxygen (full line: flux; dashed line: bulk).

clear distinction between the bulk and flux components of the longitudinal drift velocity component and diagonal elements of the diffusion tensor. This is a clear sign of the so-called explicit effects of nonconservative collisions. Since in this energy range the ionization dominates the attachment processes the distinction between the bulk and flux components is entirely caused by the explicit effects of the ionization processes. However, in the limit of the strongest magnetic field considered in this work, we see from figure 3 that the attachment rate exceeds the ionization rate and hence the negative value of the effective ionization coefficient follows. The distinctions between the bulk and flux components of the drift and diffusion are quite different during various relaxation stages. At the beginning of the relaxation process, these differences are quite large and as the relaxation process proceeds further, their evolution depend on B/n_0. For lower B/n_0, the differences between the bulk and flux values upon reaching the steady state are still remarkable while for higher B/n_0 the differences between the bulk and flux values are significantly reduced. Generally speaking, the distinction between flux and bulk components of the drift velocity vector elements is a consequence of spatially dependent nonconservative collisions resulting from a spatial variation of average electron energies within the swarm [20]. If the ionization rate is an increasing function of electron energy, electrons are preferentially created in regions of higher energy resulting in a shift in the center of mass position as well as a modification of the spread about the center of mass. For molecular oxygen and field configuration studied here, the electrons are preferentially created at the front of the swarm in the z-direction and hence the magnitude of the bulk drift component in this direction is greater than the equivalent flux component. However, for the $\boldsymbol{E}\times\boldsymbol{B}$ drift velocity component an opposite situation holds. We see for B/n_0 of 500 Hx that upon reaching the steady-state the flux dominates the bulk value. This is a clear sign that along this direction the average energy decreases and since the ionization processes dominate the attachment processes the flux value is greater than corresponding the bulk component. For B/n_0 of 1000 and 2000 Hx, there are essentially no differences between the bulk and flux values for the $\boldsymbol{E}\times\boldsymbol{B}$ drift velocity component indicating a weak spatial variation of the average energy along this direction. Our independent Monte Carlo calculations of spatially resolved transport properties support this physical picture [37].

In figure 5 we show the temporal evolution of the diagonal elements of the diffusion tensor for various ψ and B/n_0 of 100 and 1000 Hx for the Reid ramp model. The Reid ramp inelastic

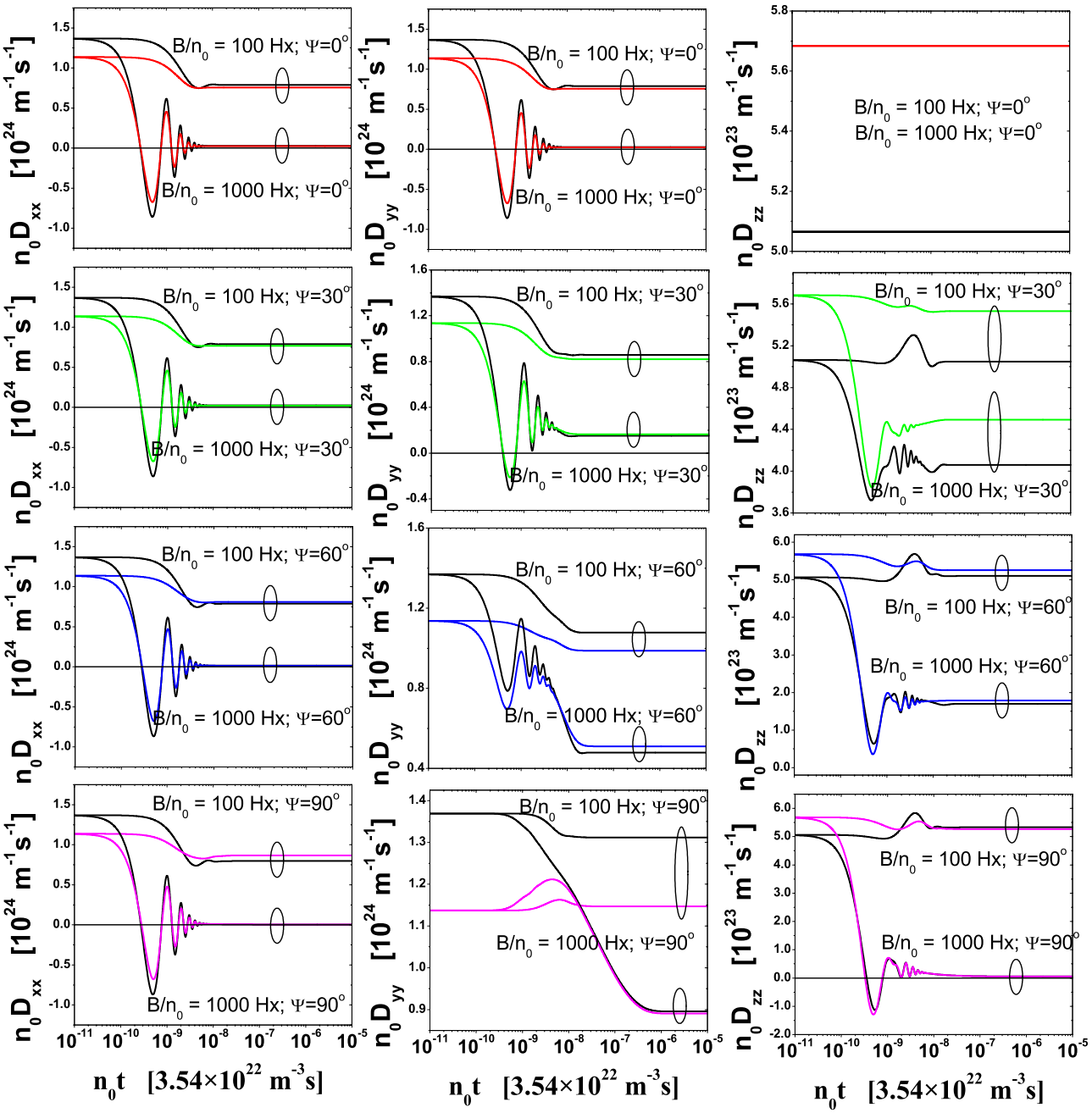

Figure 5. Temporal relaxation of the diagonal elements of the diffusion tensor for B/n_0 of 100 and 1000 Hx and various ψ for Reid ramp model (color lines: multi-term calculations; black lines: two-term approximation).

model of interaction is given by

$$\sigma_{\mathrm{m}}(\epsilon) = 6\,\text{Å}^2 \qquad \text{(elastic cross section)}$$

$$\sigma_{\mathrm{inel}}(\epsilon) = \begin{cases} 10(\epsilon - 0.2)\ \text{Å}^2, & \epsilon \geqslant 0.2\,\text{eV} \\ & \text{(inelastic cross section)} \\ 0, & \epsilon < 0.2\text{eV} \end{cases}$$

$$m_0 = 4\,\text{amu}$$

$$T_0 = 0\,\text{K}, \tag{28}$$

where m_0 and T_0 represent the mass and temperature of the neutral gas particles while ϵ has the units of eV. The Reid ramp model has been used extensively as a benchmark under steady-state [22, 21, 38, 39] and time-dependent [15, 22] conditions for a variety of field combinations, profiles, and configurations due to its well-known illustration of the failure of the two-term approximation. In figure 5 the results obtained by the two-term approximation are compared with those obtained by a multi-term theory for solving the Boltzmann equation. Similar tests have been performed by Winkler and Loffhagen [40, 41]. They employed a multi-term approach to test the validity of the two-term approximation for electrons in helium, xenon and molecular nitrogen for $\boldsymbol{E}$-field under spatially homogeneous conditions. We extend these studies into domain of spatially inhomogeneous electron swarms.

We observe a remarkable change in the relaxation profiles induced by the variation of angle between the fields. Quite

generally, the relaxation profiles for all diagonal elements of the diffusion tensor show significant sensitivity with respect to angle between the fields. We observe that the oscillatory nature of the relaxation process for $n_0 D_{xx}$ and $n_0 D_{zz}$ is enhanced as the angle between the fields increases. In particular, for parallel fields ($\psi = 0^\circ$) the diffusion coefficient along the electric field $n_0 D_{zz}$ is, as expected by symmetry, not altered by the presence of magnetic field and is equal to the magnetic field-free case value. However, as the angle between the fields increases for B/n_0 of 100 Hx, we may observe development of the additional oscillatory behavior in the relaxation profiles of $n_0 D_{zz}$ damped by collisions that exchange momentum and energy. In the limit of high B/n_0 of 1000 Hx, these oscillations lead to the existence of transiently negative diffusivity. As can be seen from figure 3, $n_0 D_{zz}$ decreases with increasing ψ for both the collision-dominated regime ($B/n_0 = 100$ Hx) and magnetic field-controlled regime ($B/n_0 = 1000$ Hx).

Similar but not identical behavior shows diffusion coefficient along the $\boldsymbol{E}\times\boldsymbol{B}$ direction ($n_0 D_{xx}$). In the collision-dominated regime and in contrast to $n_0 D_{zz}$, $n_0 D_{xx}$ increases for an increasing ψ. Further, and in contrast to $n_0 D_{zz}$, for B/n_0 of 1000 Hx the amplitude of oscillatory feature is more pronounced than that of $n_0 D_{zz}$. It should be noted that the amplitude of these oscillations increases with rising ψ while the steady-state values are a decreasing function of ψ. There is another distinct property associated with $n_0 D_{xx}$ in the limit of high B/n_0: transient negative diffusion exists for the whole range of ψ considered in this work. Conversely, $n_0 D_{zz}$ becomes transiently negative only in the limit of angles close to 90°.

Unlike $n_0 D_{xx}$ and $n_0 D_{zz}$, the temporal profiles of $n_0 D_{yy}$ show entirely different nature considering the effects of angle between the fields on the relaxation process. For parallel fields ($\psi = 0^\circ$), $n_0 D_{yy}$ is essentially equal to $n_0 D_{xx}$ due to symmetry properties [22, 21]. However, in contrast to other diagonal elements of the diffusion tensor, the oscillatory nature of $n_0 D_{yy}$ is reduced as the angle between the fields is increased. In the limit of a crossed field configuration, these profiles are monotonic. For the crossed field configuration, the Lorentz force does not act in this direction and hence there are no imprinted oscillations on the diffusion coefficient in this direction. On the other hand, for small angles between the fields, the electrons are under the action of Lorentz force producing the oscillatory relaxation profiles. As can be observed from figure 3, for B/n_0 of 1000 Hx and ψ of 0° and 30°, the Lorentz force produces negative transient diffusivity. When considering the relaxation times, we observe the following quite general feature in the relaxation profiles: for both the collision and magnetic field-controlled regime, the overall relaxation time is an increasing function of ψ. To be more specific, the overall relaxation times for non-parallel fields are on the timescale of the energy relaxation. It should be noted that this appears to be more obvious for $n_0 D_{yy}$ comparing with $n_0 D_{xx}$ and $n_0 D_{zz}$. Another striking property is the fact that the steady-state values of $n_0 D_{yy}$ monotonically increase with increasing ψ. However, one may expect a decrease in steady-state values of $n_0 D_{yy}$ for significantly higher B/n_0.

The inadequacy of the two-term approximation is clearly evident from figure 5. In particular, significant deviations between temporal profiles in the early and intermediate stages of the relaxation process can be observed. This is a clear indication that the initial distribution function and its initial evolution deviates substantially from isotropy in velocity space. In general, however, as the magnetic field and the angle between the fields increase, the deviations between the results obtained by the two-term approximation and multi-term theory are significantly diminished. This suggests that the magnetic field acts to destroy the anisotropy of the velocity distribution function, consequently inducing enhanced convergence in the l-index. A similar effect has been recently observed for electrons in CO_2 [15].

3.2. Swarms in ac electric and magnetic fields

To investigate the explicit and implicit effects of nonconservative collisions on various charged-particle transport properties in varying configurations of time-dependent electric and magnetic fields we consider the benchmark model of Lucas and Saelee [42]. The details of this model are

$$\sigma_{el}(\epsilon) = 4\epsilon^{-1/2}\ \text{Å}^2 \qquad \text{(elastic cross section)}$$

$$\sigma_{ex}(\epsilon) = \begin{cases} 0.1(1-F)(\epsilon - 15.6)\ \text{Å}^2, & \epsilon \geqslant 15.6\,\text{eV} \\ & \text{(inelastic} \\ & \text{cross section)} \\ 0, & \epsilon < 15.6\,\text{eV} \end{cases}$$

$$\sigma_I(\epsilon) = \begin{cases} 0.1\,F(\epsilon - 15.6)\ \text{Å}^2, & \epsilon \geqslant 15.6\,\text{eV} \\ & \text{(ionization cross} \\ & \text{section)} \\ 0, & \epsilon < 15.6\,\text{eV} \end{cases}$$

$$P(q,\epsilon') = 1, \quad m/m_0 = 10^{-3}, \quad E/n_0 = 10\cos\omega t, \quad \text{Td},$$
$$B/n_0 = B_0/n_0\cos(\omega t + \theta), \quad T_0 = 0 \quad \text{K}. \qquad (29)$$

The parameter F controls the magnitude of the excitation and ionization cross sections. All scattering events are assumed isotropic and the cross sections listed above are 'total' cross sections, that is, integrated over all angles. The ionization partition function $P(q,\epsilon')$ (where q is the fraction of the available energy after ionization given to the ejected electron and ϵ' is incident energy) is set equal to unity implying that all the fractions $0 \leqslant q \leqslant 1$ are equiprobable. The sensitivity of the electron transport coefficients to post-ionization energy partitioning has been studied using a Monte Carlo method [43] and multi-term theory for solving the Boltzmann equation [44]. The utility of such a model lies in the fact that the total cross section remains constant independent of the parameter F. This model thus represents a good test on the errors associated with the treatment of ionization processes as purely inelastic. It must be emphasized that it is common in the literature on ac swarms to find ionization processes simply treated as another inelastic process [45–50]. These previous publications are complemented by a comprehensive description of electron kinetics in ac electric and magnetic field when ionization processes are present.

In figure 6 we demonstrate the influence of the ionization degree F on the temporal profiles of the mean energy for different magnetic field amplitudes and phase differences between the fields for an applied reduced angular frequency

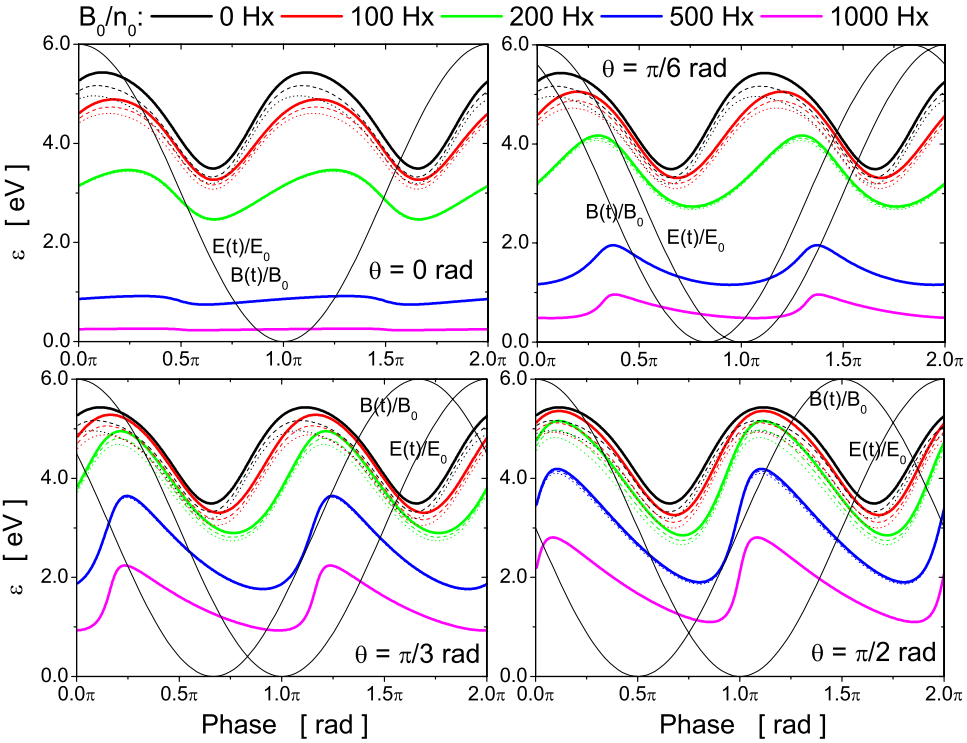

Figure 6. Temporal profiles of the mean energy as a function of the magnetic field amplitude and phase difference between the fields for the ionization model of Lucas and Saelee. The solid, dashed and dotted lines (black line: $B_0/n_0 = 0$ Hx; red line: $B_0/n_0 = 100$ Hx; green line: $B_0/n_0 = 200$ Hx; blue line: $B_0/n_0 = 500$ Hx; pink line: $B_0/n_0 = 1000$ Hx) represent the mean energy for $F = 0$, $F = 0.5$ and $F = 1$, respectively.

$\omega/n_0 = 1 \times 10^{-16}$ rad m^3 s^{-1}. We observe that mean energy decreases with increasing F for fixed B/n_0 and phase difference θ in the collision-dominated regime. After an ionization process, the remaining energy is always shared between two electrons while in the case of inelastic collision, the remaining energy is held by only one electron. As a consequence, the mean energy after ionization is lower than that after inelastic collision, a phenomenon usually called energy dilution due to ionization [51, 52]. The phenomenon of ionization cooling of the swarm is well known in dc electric and magnetic fields [16] and is shown in figure 6 to carry over directly to crossed ac electric and magnetic fields but only in the collision-dominated regime. For the magnetic field-free case we note that increasing the ionization parameter F affects not only the magnitude but also the phase of the temporal profiles. We observe that the phase lag between the mean energy and electric field decreases for an increasing ionization degree F. As B_0/n_0 increases for a fixed phase difference between the fields, the phenomenon of ionization cooling is reduced and in the limit of high B_0/n_0 it vanishes. This is a clear sign that the Maxwellization of the high energy electrons significantly reduces the ionization degree. On the other hand, as the phase difference θ increases, the phenomenon of ionization cooling is further strengthened and becomes more obvious at lower B_0/n_0 and evident at higher B_0/n_0. This follows from the behavior of the ionization rate in ac electric and magnetic fields for this particular model. One would expect an increase in ionization rate as the phase difference between the fields increases. Figure 7 verifies this prediction.

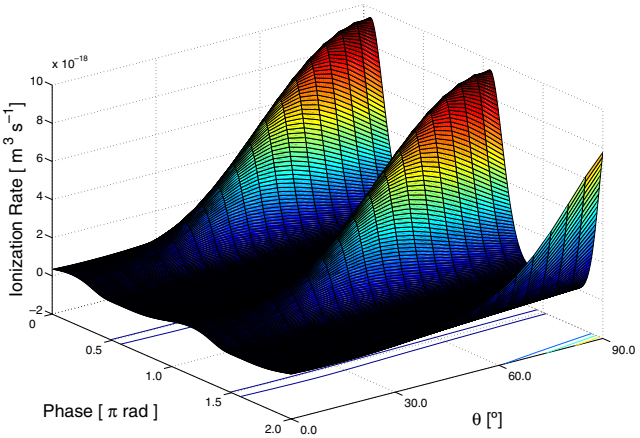

Figure 7. The three-dimensional plot of the ionization rate as a function of the phase difference θ for B_0/n_0 of 200 Hx for the ionization model of Lucas and Saelee. The parameter F is set to 0.5.

When considering the effects of the phase difference on the mean energy the following interesting points can be made. In the limit of small phase differences, the magnetic field is large when electric field peaks and electrons cannot gain much energy from the electric field—the magnetic field cools the swarm. As a consequence, the mean energy is significantly reduced. As the phase difference increases, the magnetic cooling effects are reduced, particularly in phases where electric field peaks (and magnetic field magnitude is small) and we observe that the modulation amplitude and cycle-averaged value are increased. These effects become more apparent for an increasing B_0/n_0.

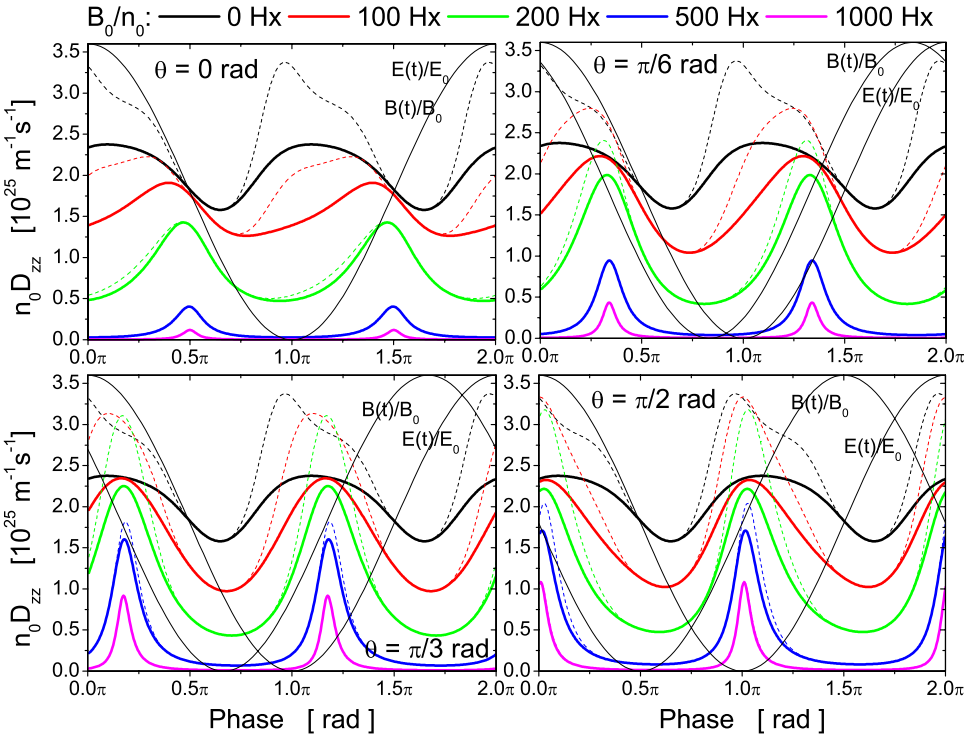

Figure 8. Temporal profiles of the bulk and flux longitudinal diffusion coefficient $n_0 D_{zz}$ as a function of the magnetic field amplitude and phase difference between the fields for the ionization model of Lucas and Saelee. The solid lines (black line: $B_0/n_0 = 0$ Hx; red line: $B_0/n_0 = 100$ Hx; green line: $B_0/n_0 = 200$ Hx; blue line: $B_0/n_0 = 500$ Hx; pink line: $B_0/n_0 = 1000$ Hx) represent the flux profiles while the dashed lines represent the bulk for $F = 0.5$.

The variation of the bulk and flux temporal profiles of the longitudinal diffusion coefficient $n_0 D_{zz}$ with the ionization degree F for four different phase differences between the fields θ and various magnetic field amplitudes B_0/n_0 is displayed in figure 8. For the magnetic field-free case, bulk longitudinal and bulk transverse diffusion coefficients are enhanced in phases where significant ionization occurs. The appearance of a spike in the bulk longitudinal diffusion profiles is indicative of an inability of the transport property to relax in combination with a non-monotonically relaxing transport property [10, 33]. The application of the magnetic field significantly affects the symmetry of both the bulk and flux components. We also note that increasing B_0/n_0 for a fixed phase difference θ, the distinction between the bulk and flux components is reduced. On the other hand, as the phase difference θ increases, the explicit effects of ionization become more evident since the ionization rate monotonically increases with θ. In general, the flux and bulk diffusion coefficients can vary substantially from one another not only in magnitude but also in the phase lags of the temporal profiles.

3.3. Spatial relaxation

In this section we extend previous work on the idealized steady-state Townsend experiment to include the explicit influence of nonconservative collisions when electric and magnetic fields are present and crossed at an arbitrary angle. The system is schematically represented in figure 9 where charged particles are emitted at a constant rate from an infinite plane source at $z = z_0$ and interact with the neutral gas under the influence

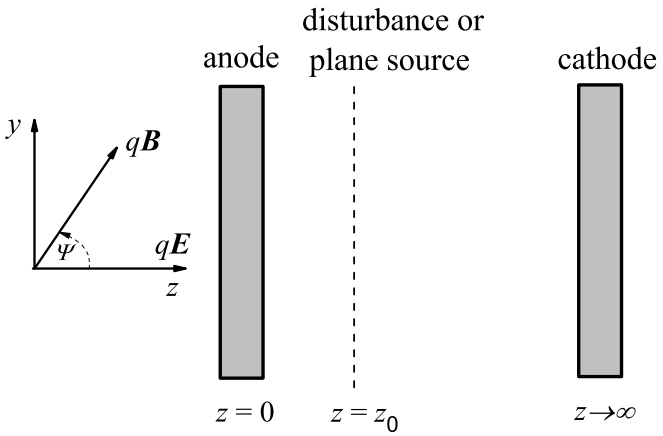

Figure 9. Schematic representation of an idealized state-state Townsend experiment.

of spatially uniform electric and magnetic fields crossed at arbitrary angles. The boundary conditions on the distribution function are detailed in [15, 22, 53]. In this section we present results for the ionization model of Lucas and Saelee defined in previous section.

In the case of an electric field only, previous work on the electron spatial relaxation revealed the complex nature of the relaxation process and associated basic mechanisms. The nature of the spatial relaxation profiles is dependent on the interplay between the power dissipated in elastic collisional processes, power dissipated in threshold collisional processes and the power deposited into the swarm by the field

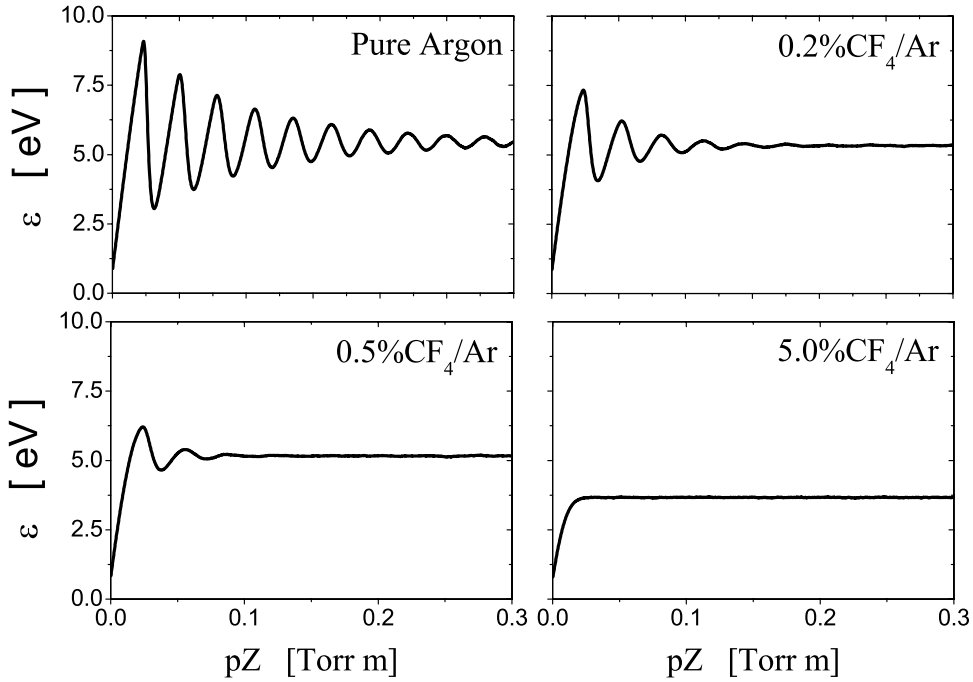

Figure 10. Spatial relaxation of the mean energy for electrons in argon–CF_4 mixtures for E/n_0 of 15 Td.

[15, 22, 53–55]. For certain gases, there exists a 'window' of electric field strengths where the relaxation profiles are damped oscillatory in nature, and outside this electric field window the profiles are monotonic. In [53] it was shown that magnetic field is able to both suppress and generate oscillatory behavior of various transport properties as well as modify the spatial relaxation distance.

Before considering the effects of a magnetic field on spatial relaxation of the electrons we present one particularly interesting set of results associated with the spatial relaxation of the electrons in gas mixtures. In figure 10 we show the spatial relaxation of the mean energy in pure argon and mixtures of argon and CF_4 at E/n_0 of 15 Td. The cross sections for argon are displayed and detailed in [14] while the cross sections for CF_4 are given in [56]. We observe that the mean energy in pure argon exhibits a damped oscillatory relaxation along a decaying profile. However, by introducing a small amount of molecular admixture (e.g. CF_4) the oscillations are firstly suppressed and then entirely quenched in the limit of higher concentration of CF_4. By introducing a molecular admixture other collision processes preferentially lower threshold vibrational excitations are introduced. These new collision processes lead to more efficient damping than elastic collisions, by virtue of larger and different energy loss mechanisms. Similar effects have been observed experimentally. As an illustrative example, on the basis of the photon-flux technique, Fletcher showed that by introducing a small amount of molecular nitrogen, luminous layers in argon can be quenched.

Figures 11 and 12 display the spatial relaxation of the mean energy and average velocity component along the z-direction for the ionization model of Lucas and Saelee ($F = 0.5$) as a function of B/n_0 in a crossed field configuration, respectively. The application of a magnetic field leads to significant changes

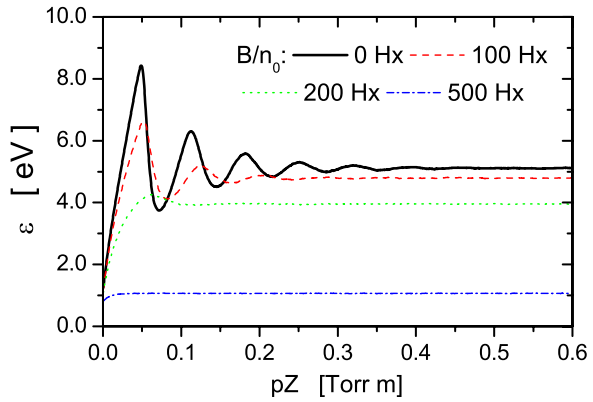

Figure 11. Spatial relaxation of the mean energy as a function of B/n_0 for the ionization model of Lucas and Saelee. The reduced electric field E/n_0 is set to 10 Td.

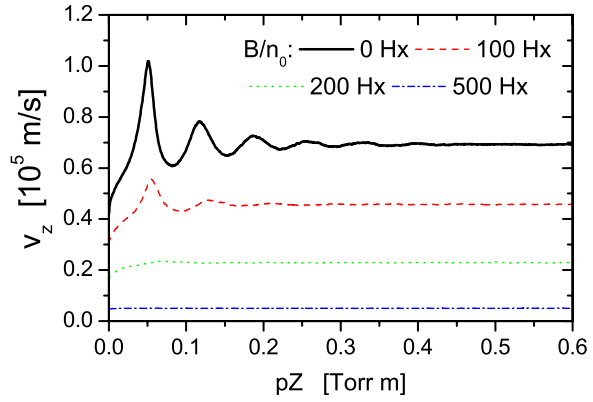

Figure 12. Spatial relaxation of the z-component of the average velocity as a function of B/n_0 for the ionization model of Lucas and Saelee. The reduced electric field E/n_0 is set to 10 Td.

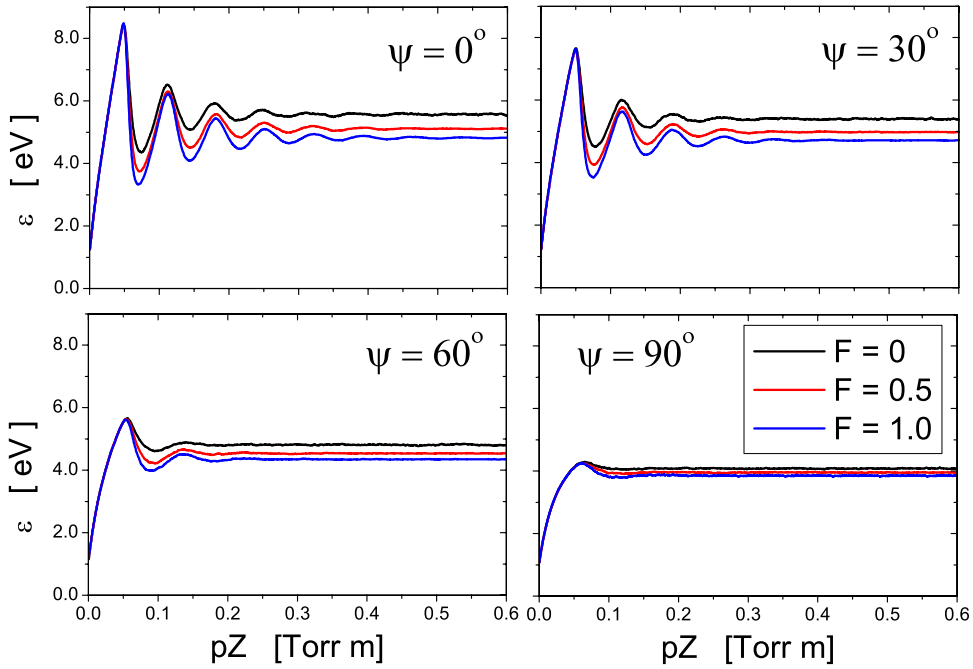

Figure 13. Spatial relaxation of the mean energy as a function of ψ for the ionization model of Lucas and Saelee and B/n_0 of 200 Hx. The reduced electric field E/n_0 is set to 10 Td.

in the relaxation profiles. When $B/n_0 = 100$ Hx, we observe that both the maximal and spatially uniform values of ε and v_z are lower than the case when $B/n_0 = 0$ Hx. This is caused by magnetic cooling effects associated with gyrations of the electrons. When B/n_0 is increased further to 200 Hx, we see that the mean energy is much less than the threshold energy of both inelastic and ionization collision processes, energy losses via these collisions are reduced, and elastic collisions are enhanced. The relaxation profiles show weak irregular oscillations which are damped in the early stage of the relaxation process. At the highest B/n_0 of 500 Hx, the effects of inelastic and ionization collisions are suppressed and the relaxation process is dominated by elastic collisions. Consequently ε and v_z relax toward a spatially uniform state monotonically.

Finally we consider the influence of the angle between the electric and magnetic fields on the spatial relaxation processes of electrons. In figure 13 we demonstrate the impact of angle between the fields on the spatial relaxation of the mean energy for the ionization model of Lucas and Saelee. For parallel fields ($\psi = 0$), the spatial relaxation profiles of the mean energy is in excellent agreement with those associated with a pure electric field. This follows from the symmetry property outlined in [21, 22]. For parallel fields, on average the electrons are traveling in the direction of the electric and magnetic field and hence the magnetic field has no explicit effect. As the angle between the fields increases, both the maximal and spatially independent (steady-state) values of ε are lower than those for parallel fields. The physical mechanism for the cooling action of a magnetic field when electric and magnetic fields are crossed at arbitrary angle under the hydrodynamic conditions is given in [16, 21, 22]. In brief, the cooling mechanism is enhanced as the component of the magnetic field perpendicular to the electric field (and hence the angle between the fields) is increased. This means that the cooling mechanism is the strongest in the limit of a crossed field configuration. Another interesting point which can be observed from these profiles is associated with the influence of nonconservative ionization collisions. First we see that the mean energy decreases when increasing F for all field orientations, except in region near the source (reduced distances less than approximately 0.05 Torr m). In region near the origin, the mean energy is directly affected by the source. Second, our careful calculation of spatially uniform values of the mean energy and average velocity revealed a clear disagreement with the same quantities obtained under the hydrodynamic conditions. A physical discussion of these phenomena is detailed in [17].

4. Conclusion

In this work we have presented briefly a systematic multi-term solution of the nonconservative Boltzmann equation in the time-dependent hydrodynamic and steady-state non-hydrodynamic regime for charged-particle swarms under the influence of spatially homogeneous electric and magnetic fields. This theory was then applied to a series of model and real gases to address the errors associated with various approximation generally found in low-temperature plasma oriented literature. In particular we have identified what we believe to be the key issues associated with the correct treatment of temporal and spatial non-locality of charged-particle swarms in varying configurations of electric and magnetic fields. In particular we have observed that magnetic field at right angle to an electric field induces damped oscillatory temporal relaxation profiles for the drift and diffusion and diffusion elements in the $\boldsymbol{E}$ and $\boldsymbol{E}\times\boldsymbol{B}$ directions. Most strikingly, the negative diffusion was observed in the

profiles of both the bulk and flux diffusion elements in these directions for sufficiently high magnetic fields. We have demonstrated the differences which can exist between the bulk and flux transport coefficients during the relaxation process and the origin of these differences. In addition to the magnetic field strength, the variation of the angle between the fields on temporal relaxation of the diagonal elements of the diffusion tensor was considered. It was found that various diffusion coefficients show different sensitivities to the magnetic field strength and angle between the fields. The errors associated with the two-term approximation for solving the Boltzmann equation are highlighted during the initial, intermediate and final stage of the relaxation process.

In the context of ac studies when electric and magnetic field are time dependent we have demonstrated how important correct treatments of nonconservative collisions and magnetic fields are. First, the treatment of ionization processes as inelastic processes can generate twofold errors in transport coefficients: it neglects the cooling action of ionization processes and neglects the effects on the center of mass associated with the generation of new electrons. It should be emphasized that the flux and bulk transport properties can vary substantially from one another, and theories which approximate the bulk transport coefficients by the flux transport properties are in general not only wrong in magnitude but also in the phase lags of the temporal profiles. These phenomena have been studied in varying configurations of electric and magnetic fields where magnetic field strength, phase difference between the fields and angle between the fields significantly alter the temporal profiles of various transport properties.

The non-hydrodynamic kinetic theory for solving the Boltzmann equation and Monte Carlo simulation code have been used to study the synergism of nonconservative collisions and magnetic field on spatial relaxation of electrons in an idealized steady-state Townsend experiment. First, we demonstrated that we were able to suppress the traditional Franck–Hertz oscillations observed in pure argon by the introduction of a small fraction of CF_4 into the system. In addition, for the first time, we have presented results that investigate the effect of varying the angle between the electric magnetic fields on the spatial evolution of the swarm when nonconservative collisions are operative. It was found that the nature of the profiles could be controlled by varying the angle: Frank–Hertz oscillations could be suppressed while oscillation periods could be modified.

Acknowledgments

SD is financially supported by IOP-EMVT under contract number 062126B. SD, RDW and RER would like to thank the support of the Australian Research Council and the Centre for Antimatter-Matter Studies, and the International Science Linkages funding scheme. Two of the authors (SD and ZLjP) were partly funded by the MNTR project 141025. It is a pleasure to acknowledge helpful discussions with Dr Bo Li, Dr Kevin Ness and Dr Zoran Raspopović.

References

[1] Makabe T and Petrović Z Lj 2006 *Plasma Electronics: Applications to Microelectronic Device Fabrication* (New York: Taylor and Francis)
[2] Lieberman M A and Lichtenberg A J 2005 *Principles of Plasma Discharges and Materials Processing* 2nd edn (New York: Wiley-Interscience)
[3] Tonks L 1937 *Phys. Rev.* **51** 744
[4] Tonks L and Allis W P 1937 *Phys. Rev.* **52** 710
[5] Heylen A E D 1980 *IEE Proc.* **127** 221
[6] Robson R E 1994 *Aust. J. Phys.* **47** 279
[7] White R D, Bobson R E and Ness K F 1999 *IEEE Trans. Plasma Sci.* **27** 1249
[8] Petrović Z Lj, Dujko S Marić D, Malović G, Nikitović Ž, Šašić O, Jovanović J, Stojanović V and Radmilović-Radjenović M 2009 *J. Phys. D: Appl. Phys.* **42** 194002
[9] Ness K F 1993 *Phys. Rev.* E **47** 327
[10] White R D, Ness K F and Robson R E 2002 *Appl. Surf. Sci.* **192** 26
[11] White R D, Dujko S, Ness K F, Robson R E, Raspopović Z and Petrović Z Lj 2008 *J. Phys. D: Appl. Phys.* **41** 025206
[12] White R D, Dujko S, Robson R E, Petrović Z Lj and McEachran R P 2010 *Plasma Sources Sci. Technol.* **19** 034001
[13] Petrović Z Lj, Raspopović Z M, Dujko S and Makabe T 2002 *Appl. Surf. Sci.* **192** 1
[14] Petrović Z Lj, Šuvakov M, Nikitović Ž, Dujko S, Šašić O, Jovanović J, Malović G and Stojanović V 2007 *Plasma Sources Sci. Technol.* **16** S1
[15] White R D, Robson R E, Dujko S, Nicoletopoulos P and Li B 2009 *J. Phys. D: Appl. Phys* **42** 194001
[16] Dujko S, White R D, Petrović Z Lj and Robson R E 2010 *Phys. Rev.* E **81** 046403
[17] Dujko S, White R D and Petrović Z Lj 2008 *J. Phys. D: Appl. Phys.* **41** 245205
[18] Boltzmann L 1872 *Wein. Ber.* **66** 275
[19] Wang-Chang C S, Uhlenbeck G E and De Boer J 1964 *Studies in Statistical Mechanics* vol II, ed J De Boer and G E Uhlenbeck (New York: Wiley) p 241
[20] Ness K F and Robson R E 1986 *Phys. Rev.* A **33** 2068
[21] White R D, Ness K F, Robson R E and Li B 1999 *Phys. Rev.* E **60** 2231
[22] Dujko S 2009 *PhD Thesis* James Cook University
[23] Kumar K, Skullerud H R and Robson R E 1980 *Aust. J. Phys.* **33** 343
[24] Ness K F and Makabe T 2000 *Phys. Rev.* E **62** 4083
[25] White R D, Robson R E, Ness K F and Makabe T 2005 *J. Phys. D: Appl. Phys.* **38** 997
[26] Robson R E 1991 *Aust. J. Phys.* **44** 685
[27] Robson R E, White R D and Petrović Z Lj 2005 *Rev. Modern Phys.* **77** 1303
[28] Dyatko N A, Napartovich A P, Sakadžić S, Petrović Z and Raspopović Z 2000 *J. Phys. D: Appl. Phys.* **33** 375
[29] Dujko S, Raspopović Z M, Petrović Z Lj and Makabe T 2003 *IEEE Trans. Plasma Sci.* **31** 711
[30] Šuvakov M, Petrović Z Lj, Marler J P, Buckman S J, Robson R E and Malović G 2008 *New J. Phys.* **10** 053034
[31] Itikawa Y, Ichimura A, Onda K, Sakimoto K, Takayanagi K, Hatano Y, Hayashi M, Nishimura H and Tsurubuchi S 1989 *J. Phys. Chem. Ref. Data* **18** 23
[32] Itikawa Y 2009 *J. Phys. Chem. Ref. Data* **38** 1
[33] Maeda K, Makabe T, Nakano N, Bzeniś S and Petrović Z Lj 1997 *Phys. Rev.* E **55** 5901
[34] White R D, Robson R E and Ness K F 1995 *Aust. J. Phys.* **48** 925
[35] Raspopović Z M, Sakadžić S, Petrović Z Lj and Makabe T 2000 *J. Phys. D: Appl. Phys.* **33** 1298

[36] Dujko S, White R D, Ness K F, Robson R E and Petrović Z Lj 2008 *J. Phys.: Conf. Ser.* **115** 012017
[37] Dujko S, White R D, Raspopović Z M, Petrović Z Lj and Makabe T 2011, in preparation
[38] White R D, Brennan M J and Ness K F 1997 *J. Phys. D: Appl. Phys.* **30** 810
[39] Raspopović Z M, Sakadžić S, Bzenić S and Petrović Z Lj 1999 *IEEE Trans. Plasma Sci.* **27** 1241
[40] Winkler R and Loffhagen D 1996 *J. Phys. D: Appl. Phys.* **29** 618
[41] Loffhagen D and Winkler R 1996 *Plasma Sources Sci. Technol.* **5** 710
[42] Lucas J and Saelee H T 1975 *J. Phys. D: Appl. Phys.* **8** 640
[43] Tzeng Y and Kunhardt E E 1986 *Phys. Rev.* A **34** 2148
[44] Ness K F and Nolan A M 2000 *Aust. J. Phys.* **53** 437
[45] Maeda K and Makabe T 1994 *Japan. J. Appl. Phys.* **33** 4173
[46] Maeda K and Makabe T 1994 *Phys. Scr.* **T53** 61
[47] Goto N and Makabe T 1990 *J. Phys. D: Appl. Phys.* **23** 686
[48] Ferreira C M and Loureiro J 1984 *J. Phys. D: Appl. Phys.* **17** 1175
[49] Ferreira C M and Loureiro J 1989 *J. Phys. D: Appl. Phys.* **22** 76
[50] Ferreira C M, Alves L L, Pinheiro L L and Sa A B 1991 *IEEE Trans. Plasma Sci.* **19** 229
[51] Robson R E and Ness K F 1988 *J. Chem. Phys.* **89** 4815
[52] Nolan A M, Brennan M J, Ness K F and Wedding A B 1997 *J. Phys. D: Appl. Phys.* **30** 2865
[53] Li B, Robson R E and White R D 2006 *Phys. Rev.* E **74** 026405
[54] Robson R E, Li B and White R D 2000 *J. Phys. B: At. Mol. Opt. Phys.* **33** 507
[55] Li B, White R D and Robson R E 2002 *J. Phys. D: Appl. Phys.* **35** 2914
[56] Kurihara M, Petrović Z Lj and Makabe T 2000 *J. Phys. D: Appl. Phys.* **33** 2146